

Effect of the phase composition and crystallite size of sol-gel TiO₂ nanoparticles on the acetaldehyde photodecomposition

Carrera-López R. ^A

*Instituto Politécnico Nacional Sección de Estudios de Posgrado e Investigación
Av. Ticomán 600, C.P. 07738, México, D.F.*

Castillo-Cervantes S.

*Instituto Mexicano del Petróleo Programa de Ingeniería Molecular
Eje Lázaro Cárdenas 152, C.P. 07730, México, D.F.*

(Recibido: 13 de octubre de 2011; Aceptado: 28 de abril de 2012)

TiO₂ nanoparticles with attractive physicochemical properties have synthesized by means of the sol-gel method and acid hydrolysis. The obtained nanoparticles have characterized by the XRD-Rietveld refinement, BET and TEM techniques, and tested in the photodecomposition of acetaldehyde. The degree of decomposition of acetaldehyde by the sol-gel TiO₂ nanoparticles was directly proportional to the brookite mass fraction but inversely proportional to the anatase mass fraction and crystallite size.

Keywords: Ti, Sol-gel, Photodecomposition, acetaldehyde, anatase, brookite

1. Introduction

Recently, a great deal of research work has carried out on the photocatalytic process with TiO₂ nanoparticles because it is a promising method for the purification and remediation of polluted air due to its low cost, environmental friendliness, high photosensitivity, non-toxicity and easy availability [1]. Nowadays, TiO₂ nanoparticles are interesting materials, since one of the most relevant targets in the VOCs control is the decomposition of low concentrations of formaldehyde and acetaldehyde in indoor environments through photoassisted reactions. Acetaldehyde has produced by the oxidation of volatile organic compounds when they are in contact with ozone in carpets, furniture, etc., and it is one of the most toxic VOCs [2]. TiO₂ nanoparticles have synthesized by many techniques, such as sol-gel method [3], chemical vapor deposition [4], solvothermal process [5], reactive sputtering [6], liquid phase deposition [7], electrochemical method [8], and hydrothermal treatment [9]. From these methods, the sol-gel method is one of the most widely used for preparing TiO₂ nanoparticles because it is possible to obtain solids in which the brookite, anatase and rutile phase composition ratios can be varied [10].

It has demonstrated the presence of anatase and rutile phases on TiO₂ nanoparticles are beneficial to enhance the photocatalytic activity [11]. In this way, the mixture of the anatase and rutile phases has been widely studied and evaluated for various applications concerning heterogeneous photocatalysis. However, the role in the photoactivity of the brookite phase present in small quantities as a by-product in the formation of TiO₂ [12, 13] has scarcely studied. The aim of the present research work was to synthesize, by means of the sol-gel method and acid hydrolysis, TiO₂ nanoparticles in which the relative

abundance of anatase (higher proportion) and brookite phases with nanometric crystallite size can be varied. The effect of the brookite/anatase ratio and that of their crystallite size on the acetaldehyde photodecomposition were investigated quantitatively.

2. Experimental

2.1 Preparation of sol-gel TiO₂ nanoparticles

In a three-neck reactor, 50 ml of either 2-propanol or ethanol (Baker 99.9 %) were mixed and put under reflux and stirring. Afterwards, the solution was adjusted to pH 2 by adding hydrochloric acid (HCl). Then, added dropwise 0.2 mol of titanium IV isopropoxide (Aldrich 99.9 %) to the solution and maintained under reflux and uniform stirring until the sol formed. After, added 3.2 mol of deionized water to the mixture until the gel obtained. The final product dried at 70 °C for 12 h, and we obtained powder. Finally, the fresh sol-gel TiO₂ nanoparticles calcined at 200 and 500 °C for 3 h.

The sol-gel catalysts labeled as follows: TiO₂-P-2000C (prepared with 2-propanol and calcined at 2000C), TiO₂-P-5000C (prepared with 2-propanol and calcined at 5000C), TiO₂-E-2000C (prepared with ethanol and calcined at 2000C) and TiO₂-E-5000C (prepared with ethanol and calcined at 5000C).

^A rcarrera@ipn.mx

Table 1. Detailed characterization of sol-gel TiO₂ nanoparticles according to XRD-Rietveld refinement.

TiO ₂ sol-gel nanoparticles	Anatase (%)	Anatase D _a (nm)	Anatase a _a (Å)	Brookite (%)	D _b (nm)	A _b (Å)	Rutile (%)	D _r (nm)	A _r (Å)
TiO ₂ -P-200°C	62.88	7.03	a=b=3.7909 c=9.4957	37.12	18.26	a=9.1676 b=5.4164 c=5.2105	Not present	Not present	Not present
TiO ₂ -P-500°C	82.67	22.04	a=b=3.7861 c=9.5061	14.90	34.02	a=9.1425 b=5.4420 c=5.1919	2.43	27.14	a=b=4.5913 c=2.9518
TiO ₂ -E-200°C	63.02	8.34	a=b=3.7884 c=9.4771	35.98	6.66	a=9.1861 b=5.4318 c=5.1938	Not present	Not present	Not present
TiO ₂ -E-500°C	81.44	20.62	a=b=3.7844 c=9.4958	18.56	14.78	a=5.1317 b=5.1308 c=5.3672	Not present	Not present	Not present

D_b: Brookite Scherrer crystallite size, A_b: Brookite lattice parameters, D_r: Rutile Scherrer crystallite size, A_r: Rutile lattice parameter.

2.2 Characterization of sol-gel TiO₂ nanoparticles

The nitrogen adsorption and desorption isotherms at -196°C were measured using Micrometrics ASAP-2000 equipment. The specific surface area and the pore size distribution (average pore diameter and mean pore volume) were measured from the adsorption isotherm using the Brunauer–Emmett–Teller method and from the desorption isotherm using the Barret–Joyner–Halender (BJH) method, respectively. The XRD patterns were obtained using a D500 Siemens diffractometer with a copper target and K α radiation ($\lambda=1.5405\text{\AA}$), operating at 35 KeV and 15mA. The reflection intensities were recorded in the 2θ interval ranging from 20 to 80°. To refine the spectra, the Rietveld analysis was applied by using the Full Prof software developed by Rodríguez Carvajal [14, 15]. The crystallite size was determined by means of the Scherrer's equation [16]. The presence of the mixture of phases in the sol-gel TiO₂ nanoparticles was analyzed by transmission electron microscopy (TEM) using a Jeol 100 CX STEM with a resolution ranging from 2 to 5Å, all analyses performed at 100 kV. From the obtained micrographs, the average crystallite size calculated by the surface/volume equation [17].

2.3 Evaluation of the photocatalytic activity

The photocatalytic activity tests for the sol-gel TiO₂ nanoparticles and bare semiconductor (Degussa 2 P25) were carried out in an automated experimental equipment at microreaction level. A quartz cell was used as photoreactor with a 365-UV lamp (UVP-Light-Sources) and a 100 $\mu\text{W}/\text{cm}^2$ intensity. The tests were carried out at ambient conditions with an acetaldehyde (CH₃CHO) concentration of 300 ppmv and 2% of dried oxygen by means of a 365-nm UV lamp. Acetaldehyde

photodecomposition studies and carbon dioxide formation have investigated by infrared spectroscopy and gas chromatography.

3. Results and Discussion

In Table 1, we reported the phase composition, crystallite size, lattice parameters and the phase composition for the sol-gel TiO₂ nanoparticles. The XRD Rietveld refining results show anatase is the main phase, with tetragonal structure; the brookite phase also presented with an orthorhombic structure; and just in the case of the TiO₂-P-500°C nanoparticles, the rutile phase exists with a tetragonal structure. By means of the empirical equation (1) developed by Zhu et al. [19], the brookite critical crystallite size (D_c) calculated:

$$D_c = \frac{192.55 D_a}{5.67 D_a + 165.01} \quad (1)$$

"D_a" and "D_b" correspond to the anatase and brookite crystallite size, and "D_c" is the transition sequence between anatase and brookite. When the crystallite size of brookite (D_b) is larger than (D_c), brookite directly transforms into rutile, whereas when D_b is smaller than D_c, brookite transforms into anatase, and then anatase into rutile. According to equation (1), the TiO₂-P-200°C nanoparticles present D_c=6.6 nm and D_b=18.26 nm (Table 1), then D_b > D_c, which can be explained by the fact that the brookite phase could grow sufficiently (34.02 nm) to transform into rutile during the calcination of these nanoparticles at 500°C. According to the aforementioned, in the TiO₂-P-500°C nanoparticles, the presence of the anatase-brookite-rutile mixture was confirmed Figure 1 (a). In the case, of the TiO₂-E-200°C nanoparticles, D_c=7.56 nm and D_b=6.66 nm were obtained (Table 1), then D_b < D_c. When these

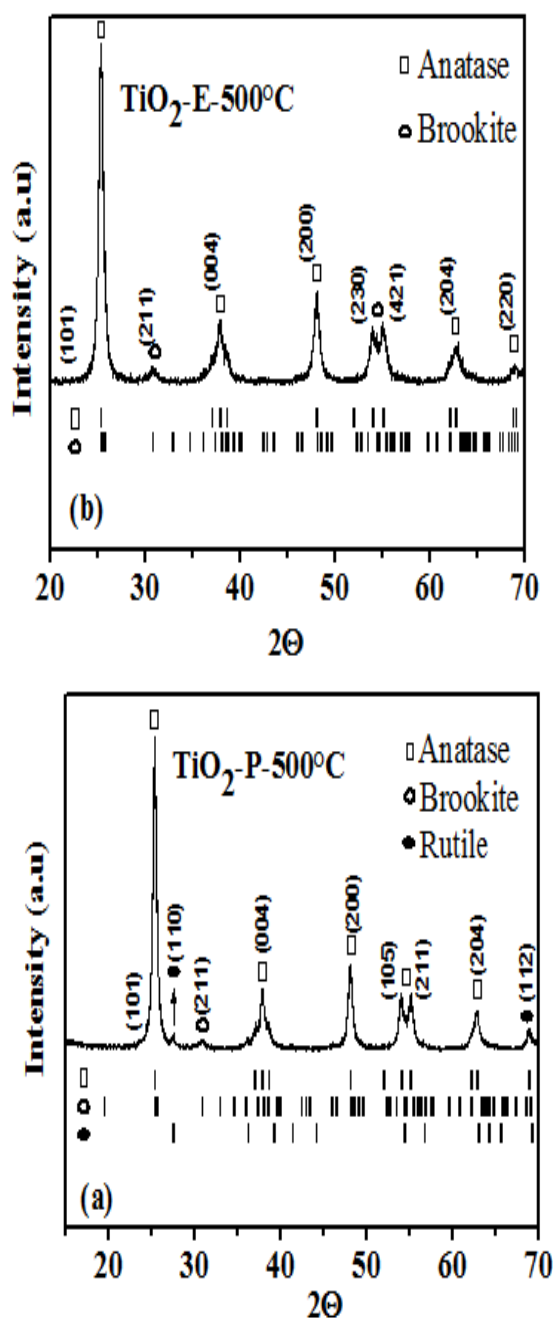


Figure 1 XRD patterns of the (a) $\text{TiO}_2\text{-P-500}^\circ\text{C}$ and (b) $\text{TiO}_2\text{-E-500}^\circ\text{C}$ nanoparticles.

nanoparticles calcined at 500°C ($\text{TiO}_2\text{-E-500}^\circ\text{C}$), the brookite phase could not grow enough (14.78 nm), transforming itself into anatase without going through the anatase-rutile transformation, Figure 1 (b).

It is hard to prepare sol-gel TiO_2 nanoparticles, with more brookite percent, and larger crystallite size by faster hydrolysis rate. Many times these nanoparticles prepared are amorphous, and easily transforms to anatase when heated above 300°C .

The surface specific area determined by the BET method in the sol-gel TiO_2 nanoparticles calcined at 200 and 500°C

listed in Table 2. It can be seen that the surface areas of the samples annealed at 200°C ($189\text{-}212\text{ m}^2/\text{g}$) are three times higher than those annealed at 500°C ($60\text{-}70\text{ m}^2/\text{g}$). Nanoparticles, characterized by lower mean pore diameters, as well as higher pore volumes, annealed at 200°C in comparison with those calcined at 500°C . The main reason for this change in the pore structure in the 500°C calcined nanoparticles attributed to sintering and/or phase transformations occurring in these sol-gel TiO_2 nanoparticles [20].

The crystalline structure and the mixture of phases present in the sol-gel TiO_2 nanoparticles observed by transmission electron microscopy (TEM), Figure 2. The mean crystallite size of the nanoparticles reported in Table 2. Through the selection, of a crystallite size in different zones of the micrographs the individual diffraction patterns obtained, and the corresponding interplanar distances were measured by means of the Digital Micrograph program which compared with the classified cards of the (J.C.P.D.S.) for TiO_2 , thus to find the crystalline structure in the corresponding direction, Table 3.

Figure 2 shows the mixtures of phases: anatase, brookite and rutile phases present in the nanoparticles, indicating the selection region in the crystallite and the corresponding diffraction pattern. A magnification of the crystallites corresponding to the anatase phase is also shown. The obtained mean crystallite sizes and the mixture of phases identified by TEM for the sol-gel TiO_2 nanoparticles are in satisfactory agreement with the XRD results (Table 2). Figure 3 shows the results of the photocatalytic evaluation of the sol-gel TiO_2 nanoparticles (see also Table 2), and those of the $\text{TiO}_2\text{-P25}$ bare semiconductor, in the acetaldehyde photodecomposition under UV irradiation as a function of time.

The sol-gel TiO_2 nanoparticles with a lower crystallite size, higher surface area and lower average pore diameter (Tables 1 and 2) present higher efficiency in the photodecomposition of acetaldehyde, Figure 3. Thermal annealing produced an increase in the crystallite size, a reduction of the specific area and a lower activity in the acetaldehyde photodecomposition. This property is remarkable in the $\text{TiO}_2\text{-E-500}^\circ\text{C}$ with efficiency of 74.3%, Figure 3. According to the aforementioned, the acetaldehyde photodecomposition is higher in the solids with high specific surface area; then, the specific surface area and crystallite size of these nanoparticles make important contributions to the acetaldehyde photodecomposition activity. Fan et al [21] reported the results indicate that the specific surface area of the sol-gel TiO_2 nanoparticles is, the more reaction sites are, which is in favor of the activity. On the other hand, with a smaller crystallite size, the number of active surface sites increases, and so does the surface charge carrier transfer rate in the photocatalytic reaction.

The selectivity to complete mineralization was followed by the formation of CO_2 . In Figure 4, it can be seen that the CO_2 formation follows a similar trend to that observed for the conversion evolution (Figure 3). The high selectivity to

CO₂ showed by the sol-gel nanoparticles is of great importance since total mineralization is one of the most

saturation of the surface is decomposed, and From the obtained results, it can be assumed that the

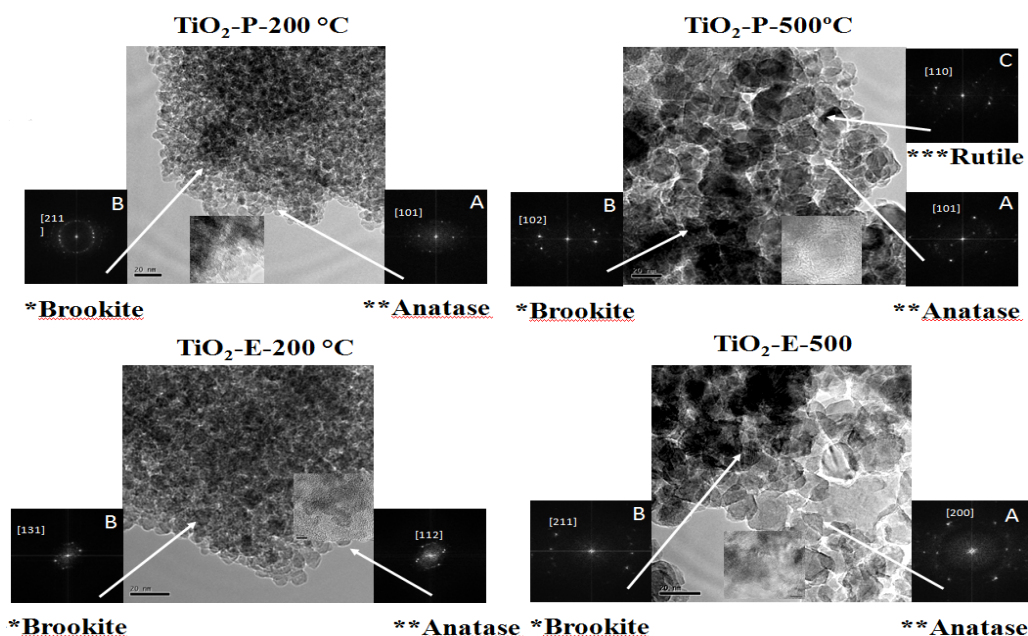


Figure 2 TEM micrographs showing the mixture of the anatase-brookite-rutile phases in the sol-gel TiO₂ nanoparticles

appreciated results. In Figure 4, it can be seen that an induction period of around 30 min is needed to identify appreciable formation of CO₂. This induction period was attributed by Sano et al., [23] to initial oxidation of acetaldehyde giving adsorbed acetic acid, which after saturation of the surface is decomposed, and then, total mineralization is reached.

The selectivity to total mineralization was followed by the formation of CO₂. In Figure 4, it can be seen that the CO₂ formation follows a similar trend to that observed for the conversion evolution (Figure 3). The high selectivity to CO₂ showed by the sol-gel nanoparticles is of great importance since total mineralization is one of the most appreciated results. In Figure 4, it can be seen that an induction period of around 30 min is needed to detect appreciable formation of CO₂. This induction period was attributed by Sano et al., [23] to an initial oxidation of acetaldehyde giving adsorbed acetic acid, which after

acetaldehyde decomposition reached by the TiO₂ nanoparticles under 365-UV light was directly proportional to the brookite mass fraction, but inversely proportional to both the anatase mass ratio and crystallite size.

The high selectivity to the formation of CO₂ in the acetaldehyde decomposition reaction depends on the intensity of light and the initial reactant concentration. Sopyan et al [22] reported that the optimum initial concentration of acetaldehyde is 300 ppm, since at this concentration the quantum yields for CO₂ production were much higher than those for acetic acid production, with a constant UV intensity.

While concentrations in the ppm range are typical for chemical stream concentration, sub ppm levels or parts per billion (ppb) concentrations are commonly indoor VOCs, (buildings, trains, vehicles, planes, etc.) VOCs [23], it would be expected to sol-gel TiO₂ nanoparticles can be effectively used for decomposing the acetaldehyde indoor,

Table 2. Specific surface area, volume and pore size of the sol-gel TiO₂ nanoparticles.

TiO ₂ sol-gel nanoparticles	Specific Surface area m ² g ⁻¹	Pore volumen cc g ⁻¹	Mean pore volume Å	Mean crystallite size (TEM) nm	Acetaldehyde photocatalytic conversion
TiO ₂ - P-200 °C	189	0.17	36	7.52	96.4
TiO ₂ - P-500 °C	60	0.11	74	22.32	80
TiO ₂ - E-200 °C	212	0.25	48	9.08	94.8
TiO ₂ - E-500 °C	72	0.16	91	20.09	74.3
TiO ₂ -Degussa-P-25	40	-	-	40	33.3

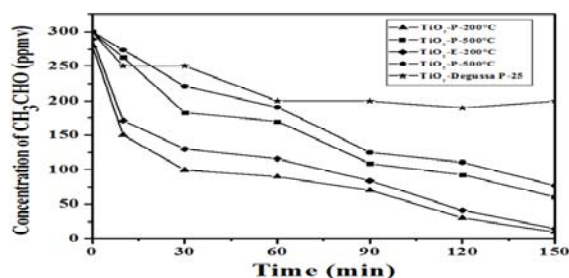


Figure 3. Acetaldehyde conversion as a function of time for the TiO₂ nanoparticles

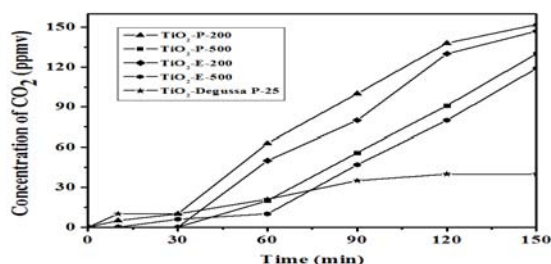


Figure 4 CO₂ selectivity in the acetaldehyde decomposition by TiO₂ nanoparticles

as it is re then, total mineralization is reached. markable that do not lose their photocatalytic efficiency at high concentrations of this pollutant (300 ppmv) due to saturation of the active sites of its specific surface area.

The high selectivity to the formation of CO₂ in the acetaldehyde decomposition reaction depends on the intensity of light and the initial reactant concentration. Sopyan et al [22] reported that the optimum initial concentration of acetaldehyde is 300 ppm, since at this concentration the quantum yields for CO₂ production were much higher than those for acetic acid production, with a constant UV intensity.

While concentrations in the ppm range are typical for chemical stream concentration, sub-ppm levels or parts per billion (ppb) concentrations are commonly indoor VOCs,

(buildings, trains, vehicles, planes, etc.) VOCs [23], it would be expected to sol-gel TiO₂ nanoparticles can be effectively used for decomposing the acetaldehyde indoor, as it is remarkable that do not lose their photocatalytic efficiency at high concentrations of this pollutant (300 ppmv) due to saturation of the active sites of its specific surface area.

According to the Rietveld-XRD results (Table 1), it can be seen that the photoactivity of the sol-gel TiO₂ nanoparticles can be related to the relative abundance of titania phases. By comparing the sol-gel TiO₂ nanoparticles, it was found that the highest acetaldehyde decomposition was obtained with the sample having the highest brookite abundance (Tables 1 and 2). The photocatalytic activity of the sol-gel TiO₂ nanoparticles can be attributed to both the crystallite size and the relative abundance of the crystalline phases; variations in these two factors modify the TiO₂ band gap, and important effects on the photocatalytic properties can be expected [24, 25]. The photocatalytic activity of the TiO₂ nanoparticles prepared by the method sol-gel consisted of anatase and brookite phases were more active than those containing anatase, brookite and rutile phases. All the sol-gel TiO₂ nanoparticles exhibited higher photocatalytic activity than TiO₂-Degussa-P-25.

Previous reports indicated that brookite may be used as an effective photocatalyst. Pure brookite nanocrystals obtained by reaction of a mixed solution of urea and TiCl₃ showed good photocatalytic properties for the degradation of acetaldehyde [26] and 4-chlorophenol [27] but the activity of these samples was relatively lower than that of TiO₂-Degussa-P-25. Di Paola et al [28] reported that the powders obtained by thermolysis of TiCl₄ in aqueous NaCl solutions consisted of anatase, brookite and rutile phases were more active than those containing only brookite and rutile phases obtained in HCl solutions. These discrepancies may be ascribed to different preparation methods and hydrolysis conditions

Table 3 Phase composition mixtures present in the sol-gel TiO₂ nanoparticles determined by TEM.

Sol.gel TiO ₂ nanoparticles	Selected crystallite	Interplanar distance (nm)	[h k l]	Phase
TiO ₂ -P-200°C	A	0.352	[1 0 1]	anatase*
	B	0.289	[2 1 1]	brookite**
TiO ₂ -P-500°C	A	0.352	[1 0 1]	anatase*
	B	0.247	[1 0 2]	brookite**
	C	0.324	[1 1 0]	rutile***
TiO ₂ -E-200°C	A	0.233	[1 1 2]	anatase*
	B	0.168	[1 3 1]	brookite**
TiO ₂ -E-500°C	A	0.189	[2 0 0]	anatase*
	B	0.289	[2 1 1]	brookite**

4. Conclusions

TiO₂ nanoparticles presenting various crystallite sizes and different compositions of the anatase-brookite phases were synthesized by the sol-gel method. The crystallite size and the weight percent composition of the anatase phase ranged from 7.03 to 22.04 nm and from 62.88 to 82.67% respectively, and from 6.66 to 34.02 nm and from 14.90 to 37.12% for the brookite phase. The photocatalytic properties of the sol-gel TiO₂ nanoparticles concerning the acetaldehyde photodecomposition were investigated in terms of the crystallite size and the presence of a mixture of the anatase and brookite phases. The highest acetaldehyde photodecomposition rate displayed by the sol-gel TiO₂ nanoparticles under 365-UV light was reached with those samples presenting the lowest crystallite size and the highest brookite phase composition. It can be concluded that the acetaldehyde decomposition was directly proportional to the brookite mass fraction and inversely proportional to the anatase mass fraction and crystallite size.

References

- [1]. O. Carp, C. L. Huisman, A. Reller, Prog. Solid State Chem. **32**, 33 (2004).
- [2]. E. Obuchi, T. Sakamoto, K. Nakano, Chem Eng Sci. **54** 1525 (1999).
- [3]. M. Zhou, J. Yu, B. Cheng, H. Yu, Mater. Chem. Phys. **93**, 159 (2005).
- [4]. T. Maekawa, K. Kurosaki, T. Tanaka, S. Yamanaka, Surf. Coat. Technol. **202**, 3067 (2008).
- [5]. C.-S. Kim, B.K. Moon, J.-H. Park, S.T. Chung, S.-M. Son, J. Cryst. Growth. **254**, 405 (2003).
- [6]. M. R. Teresa Viseu, M.I.C. Ferreira, Vacuum **52**, 115 (1999).
- [7]. J.G. Yu, H.G. Yu, B. Cheng, X.J. Zhao, J.C. Yu, W.K. Ho, J. Phys. Chem. B **107**, 13871 (2003).
- [8]. N.R. de Tacconi, C.R. Chenthamarakshan, G. Yogeewaran, A. Watcharenwong, R.S. de Zoysa, A.N. Basit, K. Rajeshwar, J. Phys. Chem. B **110**, 25347 (2006).
- [9]. D.S. Kim, S.-Y. Kwak, Appl. Catal. A Gen. **323**, 110 (2007).
- [10]. R. Carrera, A. L. Vázquez, E. Arce, M. Moran-Pineda, S. Castillo, J. Alloys Compd. **434-435** 788 (2007).
- [11]. J. C. Yu, J. G. Yu, W. K. Ho, J. C. Zhao, Chem. Commun. **19** 1942 (2001).
- [12]. N. Venkatachalam, M. Palanichamy, V. Murugesan, Mater. Chem. Phys. **104** 454 (2007).
- [13]. N. Mahdjoub, N. Allen, P. Kelly, V. Vishnyakov, J. Photochem. Photobiol. A **210** 125 (2010).
- [14]. R. Carbajal, Phys. B **192**, 55 (1993).
- [15]. X. Orlhac, C. Fillet, P. Deniard, A. M. Dulac, R. Brec, J. Appl. Cryst. **34**, 114 (2001).
- [16]. J. W. Reid, J. A. Hendry, Appl. Cryst. **39** 536 (2006).
- [17]. S. Castillo, M. Morán-Pineda, V. Molina, R. Gómez, T. López, Appl. Catal. B **15** 203 (1998).
- [18]. R. C. Nádia, F. Machado, V. S. Santana, Catal. Today **107-108** 595 (2005).
- [19]. K. R. Zhu, M. S. Zhang, J. M. Hong, Z. Yin, Mater. Sci. Eng. A **403** 87 (2003).
- [20]. A. J. Patil, M. H. Shinde, H. S. Potdar, S. B. Deshpande, Mater. Chem. Phys. **68** 7 (2001).
- [21]. X. X. Fan, T. Yu, L.-Z. Zhang, X.-Y. Chen, Z.-G. Zou, Chin. J. Chem. Phys. **20** 733 (2007).
- [22]. I. Sopyan, M. Watanabe, s. Murasawa, K. Hashimoto, J. Photochem. Photobiol. A **98** 79 (1996).
- [23]. S. Wang, H. M. Ang, M. O. Tade, Environ. International **33** 694 (2007).
- [24]. T. López, R. Gomez, E. Sanchez, F. Tzompantzi, J. Sol-Gel Sci. Technol. **22** 99 (2001).
- [25]. S. Boujday, F. Wünsch, P. Portes, J. F. Bocquet, C. Colbeau-Justin, Sol. Energy Mater. Sol. Cells **83** 421 (2004).
- [26]. J.-G. Li, C. Tang, D. Li, H. Haneda, T. Ishigaki, J. Am. Ceram. Soc. **87** 1358 (2004).
- [27]. S. Bakardjieva, V. Stengl, L. Subrt, J. Lukac, N. Murafa, D. Niznansky, K. Cizek, J. Jrkovsky, N. Petrova, J. Mater. Chem. **16** 1709 (2006).
- [28]. A. Di Paola, G. Cufalo, M. Addamo, M. Ballardita, R. Campostrini, M. Ischia, R. Ceccato, L. Palmisano, Colloid Surface A **317** 366 (2008).